11th ANKARA INTERNATIONAL AEROSPACE CONFERENCE **AIAC-2021-057**
8-10 September 2021 - METU, Ankara TURKEY

STATIC AND DYNAMIC AEROELASTIC ANALYSIS OF A VERY LIGHT AIRCRAFT

H. Gül Demirer* and Altan Kayran†
Middle East Technical University
Ankara, Turkey

ABSTRACT

Aircraft design processes need to ensure that the aircraft will be aeroelastically stable within its operational envelope. This paper presents an overview of the static aeroelastic analysis results, flutter analysis and gust response analysis results of a very light aircraft. MSC.FlightLoads and MSC.Nastran are used for aeroelastic modeling and analysis. Aerodynamic calculations are based on the Doublet-Lattice Method (DLM), the aerodynamic theory employed by Nastran for subsonic flows. DLM requires all lifting surfaces to be parallel to the free stream. In this study, aerodynamic load distribution is corrected by including the camber and the angle of incidence of the wing through the addition of initial downwash to the aerodynamic mesh. DLM correction resulted in considerable changes in trim variables and aerodynamic pressure distribution outputs of static aeroelastic analysis. It is revealed by dynamic aeroelastic stability analysis that there is no flutter issue within the flight envelope and the flutter speed is much greater than the dive speed. Dynamic response analyses indicated that the response of the aircraft dies out in a short time and the model shows a dynamically stable behavior.

INTRODUCTION

Very light aircraft are specified as single-engine air vehicles with a maximum take-off mass of not more than 750 kg, having one or two seats [EASA, 2003]. Turkish Aerospace Industries and METU have collaborated to design and develop a VLA.

Very light category aircraft are not the most prone to show aeroelastic instabilities, as they are generally not high-aspect-ratio, high-speed, highly flexible aircraft. However, aeroelastic effects need to be considered in VLA designs like all other aircraft to be certified. Indeed, the relevant certification regulation CS-VLA [EASA, 2003] requires that the aircraft is free from flutter, divergence, control surface reversal within the operational envelope. Flight envelope represents all the possible combinations of airspeed and load factors resulting from maneuver and gust encounter. Gust condition can be critical for light aircraft, as significant acceleration can be seen due to low inertial resistance [Naser, Pototzky and Spain, 2001], which can result in a load factor even greater than the limit maneuvering load factor.

*GRA in Aerospace Engineering Department, METU, Email: gul.demirer@metu.edu.tr
†Prof. in Aerospace Engineering Department, METU, Email: akayran@metu.edu.tr

In this study, the global finite element model of the VLA project is utilized as the structural model for aeroelastic analysis. By using MSC.FlightLoads and Dynamics, the aeroelastic model is generated. First, lifting surfaces and control surfaces are defined. The aerodynamic mesh is created by dividing the flat plates into elements. Infinite plate splines are employed to transfer load and displacement between the aerodynamic mesh and the structural mesh. Static and dynamic aeroelastic characteristics of the designed VLA are investigated by conducting flexible trim, flutter and discrete gust response analysis. For small commercial aircraft, the typical frequency range is considered as 0-60 Hz [Wright, Cooper, 2007]. So, modes with natural frequencies up to 60 Hz are of interest to this study's dynamic analysis.

The static aeroelastic analysis is performed for a critical flight condition. This analysis leads to the aircraft loads accounting for the deflection of the structure. Aerodynamic loads are calculated with DLM. In literature, there are studies that apply some corrections to modify the theoretically predicted aerodynamics. In [Dillinger et al., 2019], it is concluded that for lower, recompression shock-free Mach numbers, an adequate agreement of pressure distributions computed with DLM and higher-order aerodynamics can be achieved by correction for airfoil camber and twist. Considering the low-speed flight characteristics of VLA, wing incidence angle and camber are included in the aerodynamic model, and the effect of this modification on load distribution over the structure is discussed.

Later on, flutter speed and flutter frequency are found by conducting dynamic aeroelastic stability analysis.

Finally, by applying symmetrical, vertical gust conditions, the transient responses of the aircraft acceleration and the wing's internal loads are presented.

METHOD

In this work, structural and aerodynamic models of VLA are coupled to generate the aeroelastic model, and this model is used to perform three different types of aeroelastic analysis.

Structural Model

The structural model is the global finite element model of the whole aircraft, as shown in Figure 1.

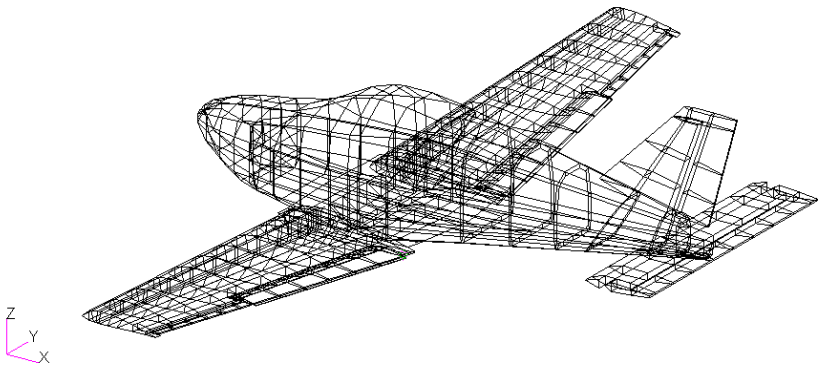

Figure 1: Structural finite element model

The VLA has a metallic airframe and structural components are made of different types of aluminum. In the structural model, linear elastic, isotropic material properties are assigned to elements. The model consists of 1439 1-D linear elements and 1693 2-D shell elements. One-dimensional elements are used to model stringers, flanges, longerons where spar webs, ribs and skin structures are modeled by triangular or quadrilateral shell elements. Besides the structural mass, concentrated mass elements are utilized to represent the mass distribution including the instruments, payload, equipment, fuel, etc. After all, the model used in the analysis has a mass of 715 kg.

Control surfaces are modeled by using multi-point constraints (MPCs) between the coincident nodes, where one of the coincident nodes is connected to the main surface and the other is to the control surface. Local coordinate systems are defined such that one of the coordinate axes is aligned with the hinge line. MPCs connecting the main surfaces and control surfaces allow the rotation about the hinge axes. Dependent and independent degrees of freedom are set accordingly to represent the connection types used in the design. In order to represent the actuator stiffness, torsional springs are modeled by CBUSH elements created between the two coincident nodes. Spring constants in the direction of rotation about the hinge axis are determined by trial and error in such a way that control surface deflection modes appear in modal analysis without coupling with the motion of other parts of the vehicle. The frequencies of the control surface modes are compared to similar airplanes' corresponding modal frequencies to check if determined stiffness values give reasonable results. [Čečrdle and Hlavatý, 2012] present mode shapes and modal frequencies of FM-250 "Vampire II" obtained by ground vibration tests and [Dimitrijević and Kovačević, 2010] list normal modes and normal frequencies of LASTA aircraft through computational modal analysis. LASTA is an aerobatic military trainer aircraft with the maximum take-off weight (MTOW) of 1210 kg, where FM-250 "Vampire II" is an ultralight sport aircraft with 600 kg MTOW. Comparison of control surface modal frequencies is given in Table 1, along with the first wing bending of vehicles.

Table 1: Comparison of modal frequencies of the VLA with the referred aircraft

Modes	VLA	LASTA Aircraft	FM-250 "Vampire II"
1st wing bending	10.056 Hz	11.397 Hz	8.575 Hz
Rudder rotation	7.328 Hz	7.316 Hz	6.941 Hz
Elevator rotation	8.171 Hz	8.140 Hz	15.06 Hz
Aileron rotation	15.368 Hz (sym) 15.139 Hz (anti-sym)	14.596 Hz (sym) -	- 14.630 Hz (anti-sym)
Flap rotation	20.105 Hz (sym) 20.568 Hz (anti-sym)	24.759 Hz (sym) 24.367 Hz (anti-sym)	- -

In static aeroelastic and gust response analysis, the symmetric boundary condition is applied at the center of gravity of the aircraft model. CG location of the finite element model is obtained by executing the grid point weight generator of Nastran. A node is created at the detected CG location and it is connected to the structural model with RBE2 rigid body elements. Two nodes are selected from each of the front and rear wing spars inside the fuselage for RBE2 connection, as shown in Figure 2. These nodes are dependent on the CG node in all degrees of freedom. Finally, single point constraint is applied to CG in translation in x and y directions and rotation about x and z directions. Furthermore, structural modal damping is not requested in flutter and gust response analyses.

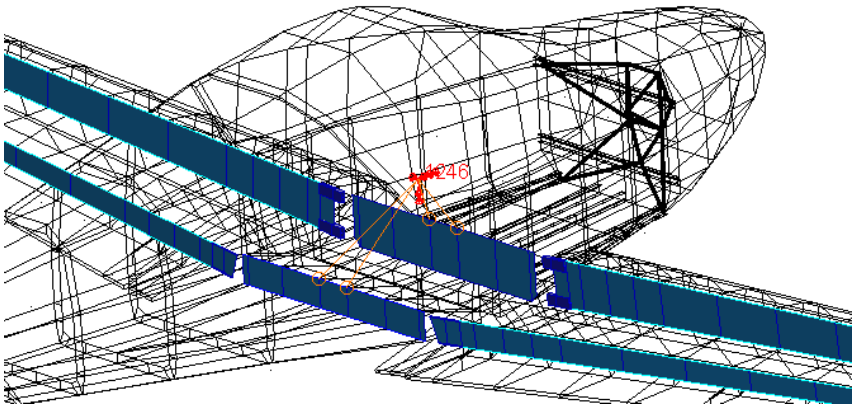

Figure 2: Connection of the CG node to the structure

Aerodynamic Model

The aerodynamic model of this study covers flat plate aero modeling of lifting surfaces. Wings, horizontal and vertical tails, and control surfaces are defined as lifting surfaces and aerodynamic boxes are created by meshing the predefined lifting surfaces. It is recommended to concentrate aerodynamic boxes near the leading edge, trailing edge and hinge lines [Rodden, Johnson, 2004]. Therefore, both uniform and biased meshing are used in order to increase mesh concentration at the critical regions. Considering the model quality, aspect ratios of the individual aerodynamic boxes are preferred to be approximately unity and less than three is acceptable for subsonic flow [Rodden, Johnson, 2004]. In this case, the aerodynamic mesh is created by taking this point into consideration and it is checked that the aspect ratio of each element does not exceed three. The fuselage is not modeled as an aerodynamic body in this case. However, in the absence of the fuselage, the gap between the wing surfaces results in unrealistic vortices at the inboard wing region [Zona Technology Inc., 2019]. Therefore, wing panels are extended to cover the gap between the wings. A similar approach is presented in [Özöztürk, Kayran and Alemdaroğlu, 2011] and the effect of bridging the gap between the wings on flutter results is discussed.

Figure 3 shows the aerodynamic mesh with and without the wing bridging panels. The mesh shown in Figure 3b consists of 1604 aerodynamic elements.

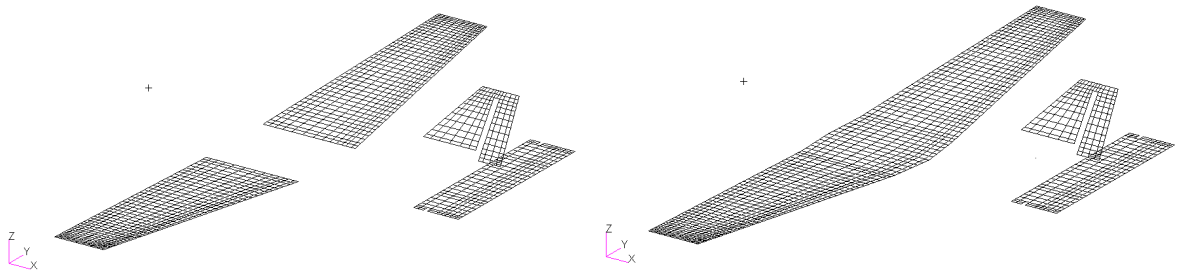

(a) Without wing bridging panels (b) With wing bridging panels

Figure 3: Aerodynamic models

Both static and dynamic analyses results presented in the following sections are obtained by covering the gap between the wings and coupling the bridging panel with the structural nodes of the front and rear spars passing through the fuselage. Beforehand, the effects of the presence of the bridging panel and splining the panel are discussed through the static trim analysis outputs.

Lifting surfaces corresponding to ailerons, flaps, elevator, and rudder are assigned as control surfaces. Control surface hinge axes are specified and the angular position limits are provided for each control surface in accordance with the design.

Aerodynamic Theory: Doublet-Lattice Method (DLM):

Doublet-Lattice aerodynamics is provided in MSC.Nastran for subsonic flows. The theory is presented in [Albano and Rodden, 1969], [Giesing, Kalman, and Rodden, 1971], and [Rodden, Giesing, and Kalman, 1972]. The theory of the DLM is based on linearized aerodynamic potential theory. The undisturbed flow is uniform and it can be steady or harmonically varying. DLM is an extended version of the steady Vortex-Lattice method for unsteady flows.

DLM is a panel method in which lifting surfaces are represented by flat panels and the panels are assumed to be parallel to the flow. Aerodynamic forces are calculated over the aerodynamic elements. DLM requires these elements to be trapezoidal boxes with sides parallel to the air-stream. For Doublet-Lattice forces, the surface normalwash boundary condition is satisfied at 75% chordwise station and spanwise center of the box while the unknown lifting pressures are assumed to be concentrated uniformly across the 25% chord line of each box [Rodden, Johnson, 2004].

In order to account for the effects of the wing incidence angle and camber, initial downwash is dictated as input on Direct Matric Input (DMI) entries of Nastran with the name W2GJ. To include

the camber effect, the initial angle of attack of each aerodynamic box is calculated at the collocation point, which is located at the 75% chord location of the boxes. The VLA wing does not have a varying twist through the span. Therefore, to account for the wing incidence effect, all aerodynamic boxes are rotated by the same angle: the incidence angle between the fuselage and the wings. Figure 4 representatively shows the local angles of attack given to aerodynamic elements for camber and incidence corrections.

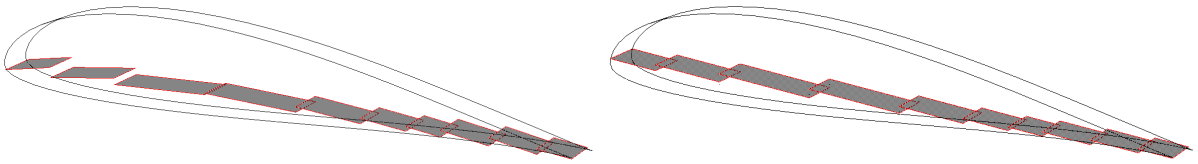

(a) Camber (b) Incidence

Figure 4: DLM correction for a chordwise strip of aerodynamic boxes

Aero-Structure Coupling

The coupling between the aerodynamic and structural meshes is established by splining. Splines enable to map the aerodynamic forces to the structural model and the structural deformations to the aerodynamic model. In this study, the Infinite Plate Spline (IPS) interpolation method is used to connect aerodynamic and structural grids. All the structural nodes located on the upper skins of lifting surfaces are selected for the transformation.

Aeroelastic Analyses

Static Aeroelastic Analysis:

Solution sequence of MSC.Nastran for static aeroelasticity, SOL 144, is used and Flexible Trim method is selected for the static aeroelastic analysis presented in this paper. It calculates the trim parameters and the resulting external loads on the aircraft.

A maneuver that is critical for the wings is specified as the flight condition of the analysis.

For static aeroelasticity, Nastran requires one or more structural degrees-of-freedom to be identified for inertia reaction [MSC.FlightLoads, 2006]. The aforementioned node located at the CG is chosen as the structural point, and translation in vertical direction and pitching about y-axis degrees-of-freedom are specified for rigid body motion to apply SUPORT boundary condition. Single point constraint is applied to the CG node in degrees-of-freedom other than vertical translation and pitching.

Flutter Analysis:

Flutter is a dynamic aeroelastic stability problem, and it requires complex eigenvalue solutions. Flutter solver of MSC.Nastran, SOL 145, provides a couple of solution methods as PK, K, PKNL, and KE. PK method is employed in this study, which computes flutter roots for density, Mach number and velocity values which are provided as input by the user [Rodden, Johnson, 2004]. The iteration process is conducted over the reduced frequency calculations and convergence of the reduced frequency is checked to finalize the iterations. In the PK method, unsteady aerodynamics is restricted to simple harmonic motion.

In this case, flutter analysis is performed for Mach 0.0, density ratio of 1.0, within the velocity range of 20 m/s to 300 m/s. The results presented in this paper are obtained from the analysis performed by including 35 roots.

Gust Response Analysis:

Discrete gust response analysis is conducted by using dynamic aeroelasticity solution sequence of Nastran, SOL 146. Gust condition is defined as described in CS-VLA [EASA, 2003] which assumes the aircraft to be subjected to symmetrical, vertical gusts in level flight. The relevant paragraph of

CS-VLA defines the gust shape and gust velocities as follows:

$$U = \frac{U_{de}}{2}(1 - cos\frac{2\pi s}{25\bar{c}}) \tag{1}$$

where U_{de} is the gust velocity specified as 15.24 m/s and 7.62 m/s at cruise and dive speeds, respectively, s is the distance penetrated into gust, and $\bar{c}$ is the mean geometric chord of the wing. Figure 5 shows the 1-cosine gust shape defined in the analyses.

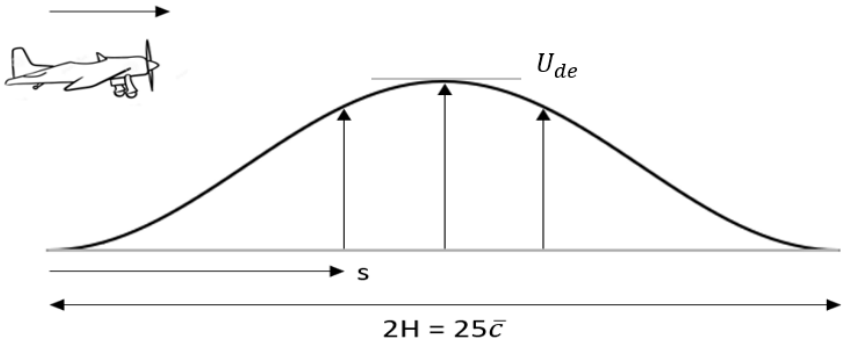

Figure 5: Discrete 1-cosine gust shape

Besides the static aeroelastic analysis, the symmetrical boundary condition is applied to the CG of the model in this analysis, as previously explained.

RESULTS AND DISCUSSION

Static Aeroelasticity

The static aeroelastic analysis is conducted for the 3.8g pull-up maneuver at 7500 feet and dive speed condition. Table 2 lists the input parameters used in the trim analysis.

Table 2: Input trim parameters

n_z	3.8 g
Mach number	0.238
Dynamic pressure	3062 Pa
Rigid body motion parameter	Angle of attack
Control surface	Elevator

Considering the flight case is a symmetric maneuver, vehicle angle of attack and elevator rotation are set as free trim parameters to be determined as a result of the static aeroelastic analysis. Three distinct models differing from each other in terms of handling the gap between the wings are analyzed and the results are given in Table 3. In the first model, wing aerodynamic panels are not extended and the gap is not covered. In the second model, the gap is covered with the wing bridging panel, but the panel is not splined to the structure. Lastly, in model 3, the wing bridging panel is coupled with the structural nodes located on the front and rear spars passing through the fuselage. When a panel connecting the wings is included in the aerodynamic model but not coupled with the structure, the aerodynamic forces produced by that panel are not transferred to the structure. Therefore, the contribution of this bridging panel is not accounted for in the aerodynamic forces that will balance the inertia in the trim analysis. This explains the difference between the results of the second and the third models. In the case of model 3, the trim condition can be satisfied at lower angles with the contribution of the aerodynamic forces arising from the bridging panel. Even though the bridging panel itself is not included in trim calculations when it is not splined, the presence of the panel

changes trim results. This can be seen by comparing the results of models 1 and 2 in Table 3. The change in the pressure distribution over the inboard sections of the wings due to the presence of the bridging panel is illustrated in Figure 6. In model 2, the bridging aerodynamic panel prevents the unrealistic aerodynamic solution due to the gap at the wing roots. Therefore, model 1 is not an option due to unacceptably high trim angles. In this study, aerodynamic modeling of the fuselage is not performed. In order to account for the aerodynamic contribution of the fuselage, model 3 is preferred to be used in the subsequent analyses.

Table 3: Trim results for different wing bridging approaches

	model 1: no bridge	model 2: bridge not splined	model 3: bridge splined
Trim angle of attack	13.1 °	9.9 °	7.9 °
Elevator rotation	21.1 °	5.2 °	3.4 °

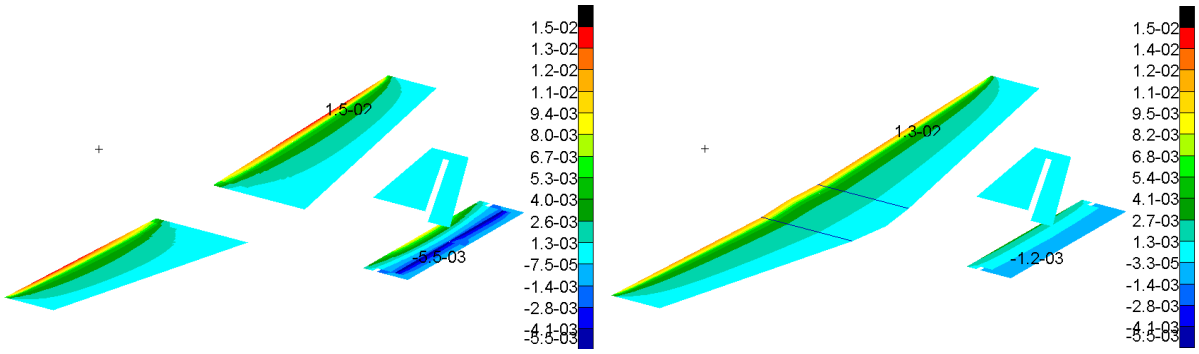

(a) model 1 (b) model 2

Figure 6: Pressure distributions [MPa] over the aerodynamic meshes of models 1 and 2

Having decided to proceed with the aeroelastic model 3, first, an analysis is performed without any intervention to the aerodynamic theory and the results of this analysis are given as the ones without DLM correction. Then, the slope of each aerodynamic element is calculated from the mean camber-line equation of the wing profile and it is added to the wing incidence angle, which is constant for all wing elements. Airfoil SD7062 with the maximum camber of 3.5% at 38.8% chordwise location is used in the VLA wings and the incidence angle between the wing and the fuselage is 1.5°. Results obtained with this approach are presented as the ones with DLM correction.

Table 4 indicates how trim variables are affected when initial downwash is included in the aerodynamic calculations. When the incidence and camber of the wings are taken into account, wings generate more lift and the aerodynamic forces can balance the inertia of the aircraft at lower values of angle of attack and elevator rotation.

Table 4: Resultant trim variables

	Without DLM correction	With DLM Correction
Trim angle of attack	7.9 °	4.3 °
Elevator rotation	3.4 °	2.1 °

Deformation of the aerodynamic mesh is one of the outputs to be checked. The aerodynamic mesh is deformed by transferring the displacement of structural nodes with the help of splines. Figure 7 depicts the deformation of the aerodynamic model when DLM correction is applied. The maximum displacement of 86 mm seen at the wing tip reduces to 79 mm for the case in which initial downwash is ignored.

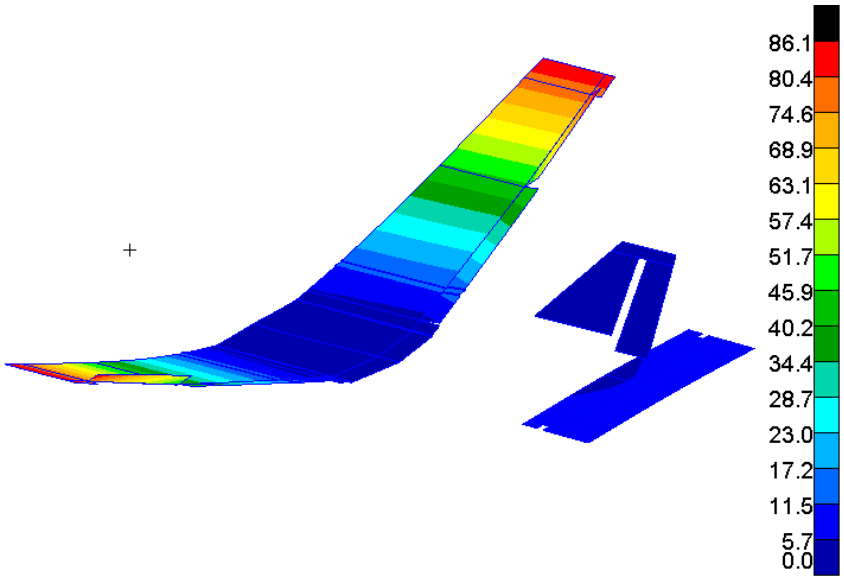

Figure 7: Deformed aerodynamic mesh [mm] with DLM correction

Pressure over the aerodynamic mesh is visualized in Figure 8. These plots enable to see the effect of wing incidence and camber on the pressure distribution and also to compare the rigid and elastic parts of the aeroelastic pressure. The aerodynamic pressure distribution calculated without taking the deformation of the model into account is given as the rigid component of aeroelastic pressure, where the elastic component indicates the incremental pressure due to the deformation of the elastic structure. The elastic component of pressure is lower in magnitude since it represents the additional effect coming from the flexibility. For both of the cases with or without DLM correction, it can be seen that the negative elastic pressure values are more significant in magnitude than the positive ones. A different distribution in the aileron region from the rest of the wing draws attention in Figures 8c and 8d. This is because of the motion of that surface due to the flexibility in the aileron connection. The elastic pressure component becomes more remarkable when DLM correction is applied. Moreover, in Figure 8c, the elastic component of the pressure distribution over the wings is relatively uniform, while variation in distribution can be seen in Figure 8d when DLM correction is applied. Lastly, by looking at the major component of pressure from Figures 8a and 8b, it can be observed that the maximum pressure value seen at the wing leading edge decreases with DLM correction. However, moderate pressure regions shown in greens and light blues expand in chordwise direction when wing incidence and camber effect are included. Furthermore, the distribution pattern over the wings is not followed by the bridging panel in 8b. This arises from the fact that DLM correction is applied only to the wing panels.

3.8g pull-up maneuver at dive speed is a critical flight condition for the wings. Von Mises stress distribution over the wing structure is plotted in Figure 9. It can be seen that for both cases, stress is concentrated at the wing root, around the front spar. DLM correction slightly changes the stress distribution pattern. In addition, the maximum stress value is increased from 113 MPa to 125 MPa at the same location. In Figure 9b, around the mid-span of the wing, the stress contour concentrated about the front spar has a tendency to expand towards the trailing edge when compared to Figure 9a. This can be explained by the effect of DLM correction on the pressure distribution of the wing, as discussed earlier.

Flutter

Flutter analysis is performed at the sea level, incompressible flow, i.e., Mach 0.0 condition using the third model, which involves the splined panel covering the gap between the wings. Firstly, modal analysis is carried out and the frequency of the first elastic mode is found to be 7 Hz. Dimensionless parameter reduced frequency is provided in a range calculated by taking the maximum and the

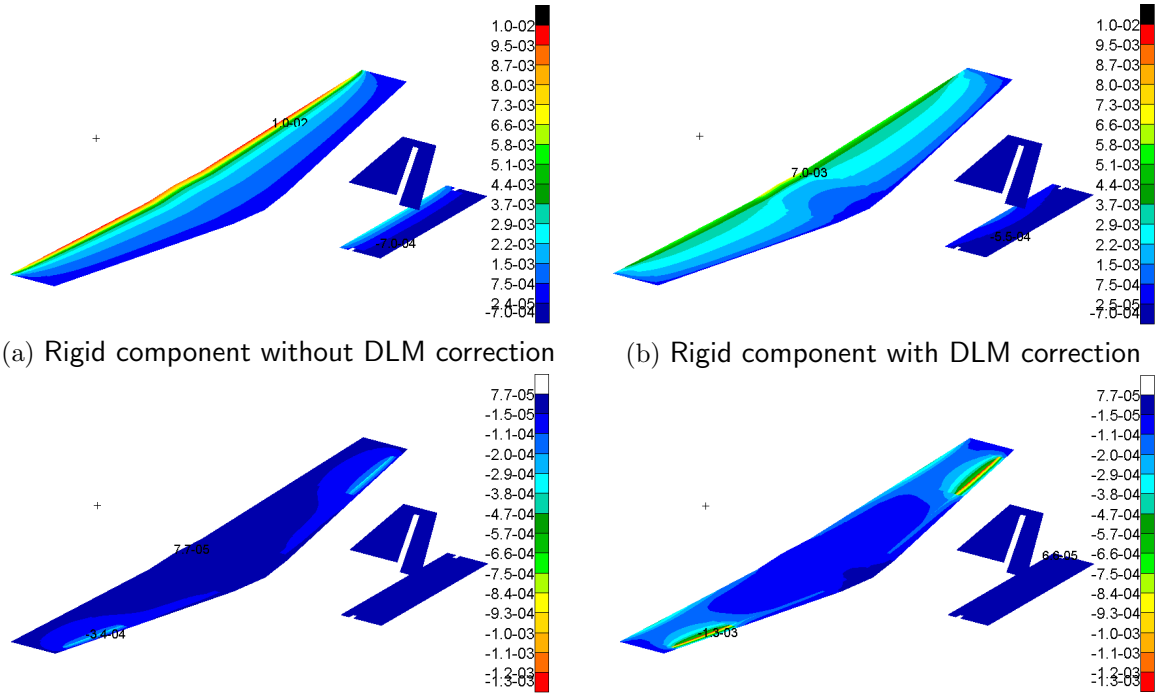

(a) Rigid component without DLM correction

(b) Rigid component with DLM correction

(c) Elastic component without DLM correction

(d) Elastic component with DLM correction

Figure 8: Rigid and elastic components of aeroelastic pressure in [MPa] with and without DLM correction

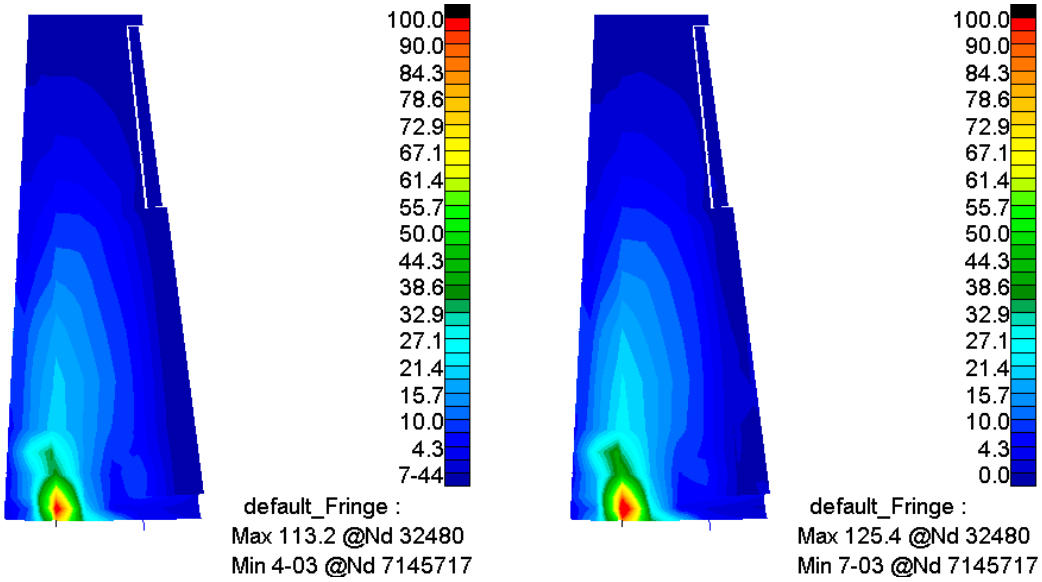

(a) Without DLM correction

(b) With DLM correction

Figure 9: Von Mises stress distribution over the wing structure [MPa]

minimum frequencies as 5 Hz and 60 Hz, the minimum and the maximum velocities as 20 m/s and 300 m/s. The dive speed of the VLA is 70.7 m/s; however, the velocity range is extended to 300 m/s to detect flutter occurrence. No structural damping is included in the analysis.

Flutter solution by the PK method ends up with complex roots in which the imaginary part represents the frequency and the real part corresponds to damping. Roots with positive real part, $g > 0$, point out an instability in the system. Therefore, sign change of damping is watched for in flutter output and crossing of g=0 while damping passes from negative to positive is remarked as the flutter

boundary. Figure 10 shows the change in damping and frequency within the velocity range for the unstable mode and indicates the flutter speed and the corresponding frequency as 178.7 m/s and 47.6 Hz, respectively.

At 160 m/s and 170 m/s, damping and frequency values fall outside the trends of the rest of the curves. When the mode shapes at that frequencies are checked, it is seen that they are not local modes to be excluded in the dynamic analysis. Therefore, flutter plots are given without omitting these extreme data points corresponding to aircraft level modes.

The velocity at which the damping is exactly equal to zero is found as 178.7 m/s by linear interpolation. The solution is obtained for Mach 0.0 at the sea level condition. The 178.7 m/s speed corresponds to Mach 0.526 at sea level, which does not match with the input Mach number. So, the flutter analysis is repeated with the input Mach number of 0.526 and the iterative analyses are conducted until the input and resultant Mach numbers converge. Hence, the matched flutter solution is found as 199.4 m/s, Mach 0.586 at sea level.

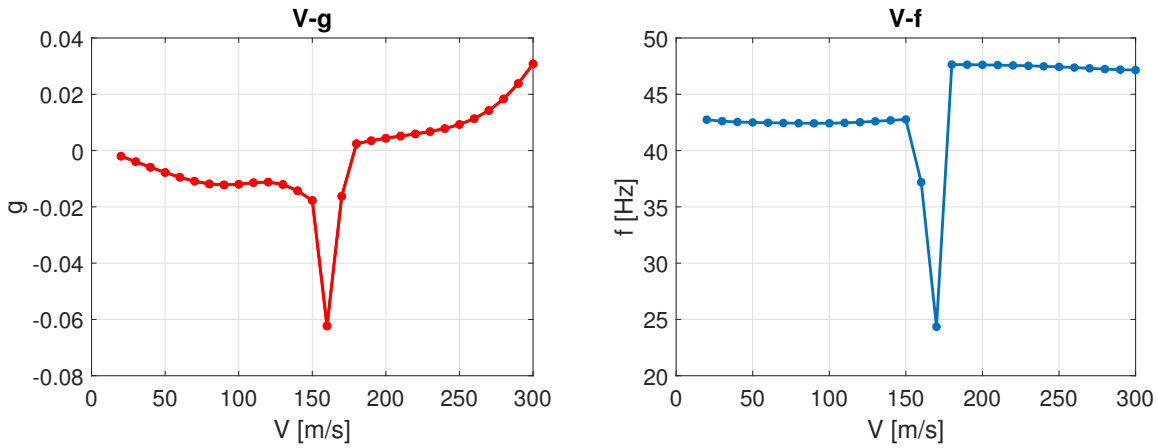

(a) Velocity vs Damping (b) Velocity vs Frequency

Figure 10: Variation of damping and frequency with the velocity for the unstable mode

The flutter mode shape is illustrated in Figure 11. The flutter mode shape involves the coupling of the in-plane and out-of-plane bending of the wings together with the symmetric horizontal tail bending and in-plane vertical tail bending.

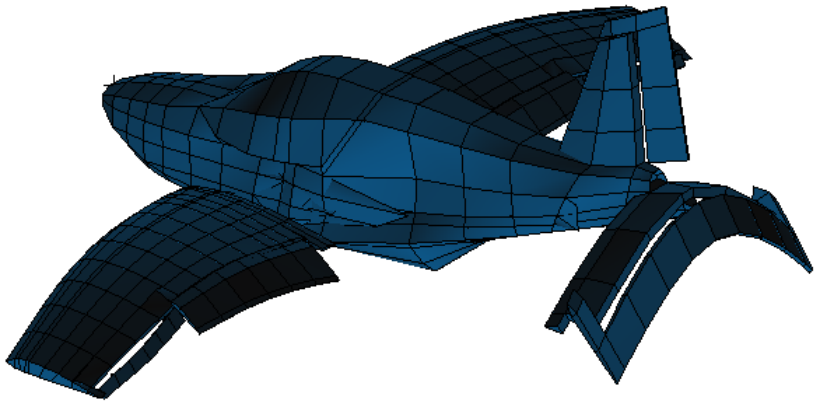

Figure 11: Flutter mode shape

Discrete Gust Response

Discrete (1-cosine) waveform gust with a single gust gradient length of H=12.5$\bar{c}$ at 7500 feet altitude is considered in this study. Figure 12 illustrates the gust profile at cruise and dive speed conditions. The indicated cruise and dive airspeeds are 56.6 m/s and 70.7 m/s, respectively. As stated in CS-VLA [EASA, 2003], gust velocity at the cruise condition is 15.24 m/s, whereas it decreases to 7.62 m/s at the dive condition. Transient response of the model to the 1-cosine gust is given in Figures 13 and 15.

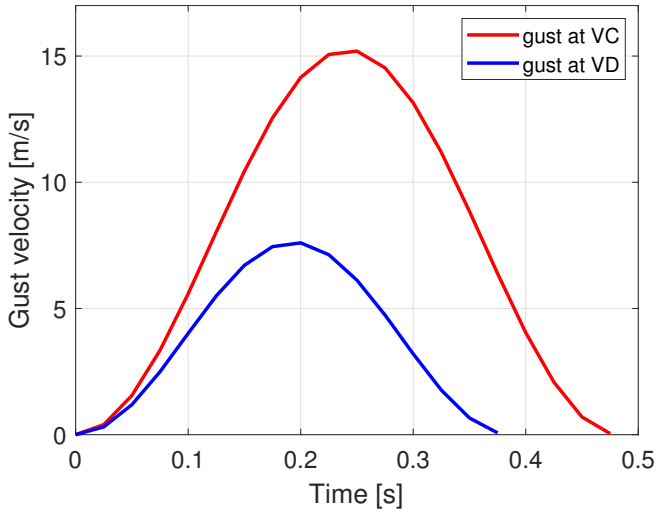

Figure 12: 1-cosine gust profile at cruise and drive speeds

Acceleration of the airplane is a desired output of gust response analysis and it is highly dependent on the weight of the model. Vertical acceleration response at the CG of the VLA model along time is plotted in Figure 13 for up and down gusts encountered at cruise and dive speeds. As a result, positive 4.15g and negative 2.15g maximum total accelerations are observed for the gusts at the cruise speed. As seen in Figures 13 and 15, gust input is provided such that the air vehicle encounters the gust at t=0.2 seconds. For all types of results, analyses conducted at the cruise speed resulted in higher responses than that of dive speed since gust velocity at V_C is higher, as shown in 12. When only the additional contribution due to gust is considered, positive and negative gusts result in responses equal in magnitude and opposite in sign. However, the corresponding values at the steady flight are added to the gust responses and plotted here. Therefore, in the response plots, the values before t=0.2s, the instant gust initiates, represent the results obtained from 1g steady level flight.

Since a vertical gust is considered, vertical shear force and vertical bending moment responses are also investigated at the wing root. For the wing root shear force, a quadrilateral shell element located at the front spar web is selected. To check the bending moment effect, the change in the axial force of the bar element located at the front spar upper flange is examined. In Figure 14, structural entities selected to investigate the internal loads at the wing root are shown.

As seen in Figure 15, positive gust causes a negative axial force response initially; since the upper flange element is examined, it undergoes compression. It can be concluded that the loading increases significantly compared to the initial steady values in a short time and then, response dies out in about 1.5 seconds.

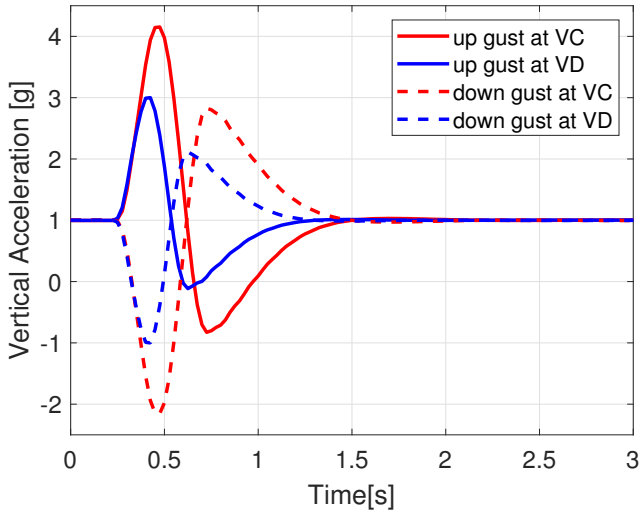

Figure 13: Gust response of vertical acceleration at the CG for up and down gusts at cruise and drive speeds

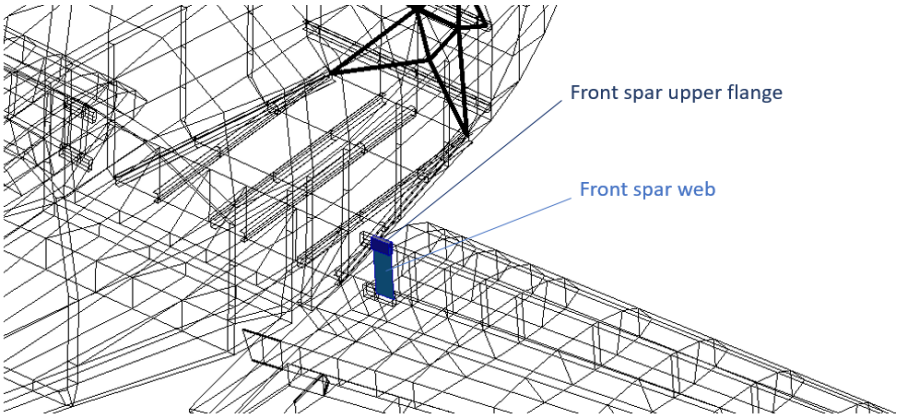

Figure 14: Front spar upper flange and web elements at the wing root

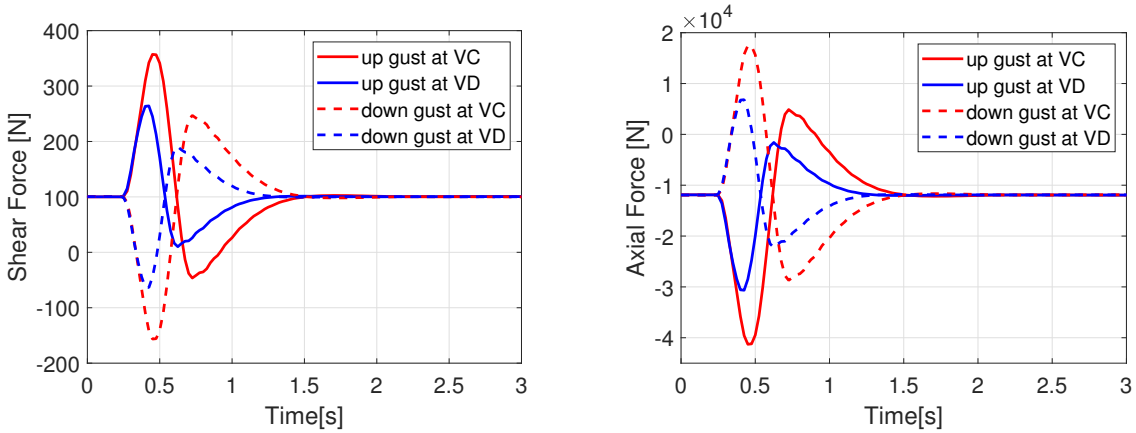

(a) Shear force at wing root front spar web (b) Axial force at wing root front spar upper flange

Figure 15: Gust response of the internal loads at wing root

CONCLUSIONS

Static aeroelastic, dynamic aeroelastic stability and dynamic response characteristics of a very light aircraft are investigated in this paper by utilizing MSC.FlightLoads and MSC.Nastran.

In static aeroelasticity, without the need to use another external program for aerodynamic calculations, distributed aerodynamic pressure loads are obtained to analyze the structure for a critical case. Static aeroelasticity leads to more realistic results as the aerodynamic loads take the structural deformations into account. Incremental pressure due to elasticity is compared to the rigid part of the aeroelastic pressure and it is concluded that the flexible aileron connection dominates the elastic pressure component. The aerodynamic solver of the Nastran for subsonic flows, DLM, has some limitations, such as assuming all lifting surfaces to be parallel to the free stream. In this study, camber and incidence of the wing are included in aerodynamic calculations by imposing initial downwash to the wing aerodynamic mesh. When wing incidence angle and camber is considered, greater aerodynamic forces are generated over the wings and the aircraft is trimmed at a lower angle of attack and elevator rotation. The maximum value of the pressure calculated on the aerodynamic mesh is decreased and the pressure distribution over the wings is changed significantly.

With dynamic aeroelastic stability analysis, matched flutter speed is found as 199.4 m/s. CS-VLA [EASA, 2003] requires analysis to show that the aircraft is free from flutter for all speeds up to 1.2 V_D where V_D of the analyzed VLA is 70.7 m/s. It is shown in this study that the flutter speed is far beyond the flight envelope.

In dynamic response analysis, discrete (1-cosine) waveform, positive and negative gusts at cruise and dive flight speeds are considered and transient response of the aircraft is given. It is seen that gust encounters at V_C condition result in more critical responses. The maximum positive acceleration response is observed as 4.15 g for upward gust at V_C and the absolute maximum negative acceleration response at -2.15g for downward gust at V_C. Considering that the positive and negative limit maneuvering load factors of the VLA are 3.8g and -1.5g, respectively, gust load factors at V_C are found to be more critical. Finally, by checking the gust response of the internal loads at the wing root, it is seen that when gust initiates, internal loads increase significantly compared to the initial steady values and then responses die out, as in the acceleration response, and the model exhibits dynamically stable behavior.

References

Albano, E. and Rodden, W.P. (1969) *Doublet-Lattice Method for Calculating Lift Distributions on Oscillating Surfaces in Subsonic Flows*, AIAA J., Vol. 7, pp. 279-285, 1969

Čečrdle, J. and Hlavatý V. (2012) *Aeroelastic Certification OF Light Sport Aircraft According "LTF" Regulation*, Engineering Mechanics, May 2012

Dillinger, J.K.S., Abdalla, M.M., Meddaikar, Y.M. and Klimmek T. (2019) *Static aeroelastic stiffness optimization of a forward swept composite wing with CFD-corrected aero loads*, CEAS Aeronautical Journal, 2019

Dimitrijević, J. and Kovačević, P. (2010) *Computational Modal Analysis of the LASTA Aircraft*, Scientific Technical Review, Vol.60, No.1, pp.60-69, 2010

EASA (2003) *Certification Specifications for Very Light Aeroplanes CS VLA*, Decision No 2003/18/RM of the Executive Director of the EASA (2003)

Giesing, J.P., Kalman, T.P. and Rodden, W.P. (1971) *Subsonic Unsteady Aerodynamics for General Configurations; Part I, Vol. I - Direct Application of the Nonplanar Doublet-Lattice Method.*, Air Force Flight Dynamics Laboratory Report No. AFFDL-TR-71-5, Part I, Vol. I, 1971

Giesing, J.P., Kalman, T.P. and Rodden, W.P. (1972) *Subsonic Unsteady Aerodynamics for General Configurations - Application of the Doublet-Lattice-Method and the Method of Images to Lifting-Surface/Body Interference.*, Air Force Flight Dynamics Laboratory Report No. AFFDL-TR-71-5, Part II, Vol. I, 1972

Giesing, J.P., Kalman, T.P. and Rodden, W.P. (1972) *Subsonic Unsteady Aerodynamics for General Configurations - Computer Program N5KA*, Air Force Flight Dynamics Laboratory Report No. AFFDL-TR-71-5, Part II, Vol. II, 1972

Giesing, J.P., Kalman, T.P. and Rodden, W.P. (1972) *Subsonic Steady and Oscillatory Aerodynamics for Multiple Interfering Wings and Bodies*, J. Aircraft, Vol. 9, pp. 693-702, 1972

MSC.FlightLoads (2006) *MSC.FlightLoads and Dynamics User's Guide Version 2006*, MSC.Software Corporation 2006

Naser, A.S., Pototzky, A.S. and Spain, C.V. (2001) *Response of the Alliance I Proof-of-Concept Airplane Under Gust Loads*, NASA / CR-2001-210649, March 2001

Özöztürk, S., Kayran, A. and Alemdaroğlu, N. (2011) *On the Design and Aeroelastic Stability Analysis of Twin Wing-Tail Boom Configuration Unmanned Air Vehicle*, AIAA, April 2011

Rodden, W.P. and Johnson, E.H. (2004) *MSC.NASTRAN Aeroelastic Analysis User's Guide*, MSC.Software Corporation 2004

Wright, J.R. and Cooper, J.E. (2007) *Introduction to aircraft aeroelasticity and dynamic loads*, John Wiley 2007

Zona Technology Inc. (2019) *ZAERO User's Manual, Version 9.3*, Zona Technology Inc. 2019